

'Glocal' Robustness Analysis and Model Discrimination for Circadian Oscillators

Marc Hafner^{1,2,3}, Heinz Koepl^{1,4}, Martin Hasler¹, Andreas Wagner^{2,3,5,6*}

1 School of Computer and Communication Sciences, Ecole Polytechnique Fédérale de Lausanne, Lausanne, Switzerland, **2** Department of Biochemistry, University of Zurich, Zurich, Switzerland, **3** Swiss Institute of Bioinformatics, Lausanne, Switzerland, **4** Plectix Biosystems, Somerville, Massachusetts, United States of America, **5** The Santa Fe Institute, Santa Fe, New Mexico, United States of America, **6** Department of Biology, University of New Mexico, Albuquerque, New Mexico, United States of America

Abstract

To characterize the behavior and robustness of cellular circuits with many unknown parameters is a major challenge for systems biology. Its difficulty rises exponentially with the number of circuit components. We here propose a novel analysis method to meet this challenge. Our method identifies the region of a high-dimensional parameter space where a circuit displays an experimentally observed behavior. It does so via a Monte Carlo approach guided by principal component analysis, in order to allow efficient sampling of this space. This 'global' analysis is then supplemented by a 'local' analysis, in which circuit robustness is determined for each of the thousands of parameter sets sampled in the global analysis. We apply this method to two prominent, recent models of the cyanobacterial circadian oscillator, an autocatalytic model, and a model centered on consecutive phosphorylation at two sites of the KaiC protein, a key circadian regulator. For these models, we find that the two-sites architecture is much more robust than the autocatalytic one, both globally and locally, based on five different quantifiers of robustness, including robustness to parameter perturbations and to molecular noise. Our 'glocal' combination of global and local analyses can also identify key causes of high or low robustness. In doing so, our approach helps to unravel the architectural origin of robust circuit behavior. Complementarily, identifying fragile aspects of system behavior can aid in designing perturbation experiments that may discriminate between competing mechanisms and different parameter sets.

Citation: Hafner M, Koepl H, Hasler M, Wagner A (2009) 'Glocal' Robustness Analysis and Model Discrimination for Circadian Oscillators. PLoS Comput Biol 5(10): e1000534. doi:10.1371/journal.pcbi.1000534

Editor: Jason A. Papin, University of Virginia, United States of America

Received: April 22, 2009; **Accepted:** September 15, 2009; **Published:** October 16, 2009

Copyright: © 2009 Hafner et al. This is an open-access article distributed under the terms of the Creative Commons Attribution License, which permits unrestricted use, distribution, and reproduction in any medium, provided the original author and source are credited.

Funding: All authors are grateful to SystemsX.ch grant for IPhD Project "Quantifying Robustness of Biochemical Modules to Parametric and Structural Perturbations". HK acknowledges the support from the Swiss National Science Foundation (SNF), grant 200020-117975/1. AW acknowledges support from SNF grants 315200-116814 and 315200-119697, as well as from the SystemsX.ch RTD project "Coping with uncertainty: Towards an integrated understanding of nutrient signaling, regulation and metabolic operation". The funders had no role in study design, data collection and analysis, decision to publish, or preparation of the manuscript.

Competing Interests: The authors have declared that no competing interests exist.

* E-mail: aw@bioc.unizh.ch

Introduction

Biologists' qualitative reasoning about outcomes of experiments show inherent limitations. Mathematical models of cellular processes, such as signaling, cell-cycle regulation, or circadian rhythmicity [1,2] can compensate for these limitations. Such models are often systems of ordinary differential equations, whose state variables represent the molecules that take part in a process. The interactions between molecules are encapsulated in the differential equations themselves, where multiple biochemical parameters determine rates at which molecules are synthesized or degraded, at which they associate, dissociate, or are transformed into other molecules. Although some data on a cellular process often exists to inform such models, substantial uncertainty often remains about which molecular interactions occur in it, and about values of the parameters governing these interactions [3].

When given two models for the same cellular process, which one is better in the face of such uncertainty about model structure and parameters? Traditionally, this question has often been approached by model calibration [4]. Here, a model is judged superior if there exist parameters (in its usually high-dimensional

parameter space) that allow the model to mimic biologically observed behavior more closely than other models. This approach fails in the common situation where parameters are underdetermined by model behavior and thus many parameter sets exist that match the behavior equally well [5]. That this deficiency is particularly pronounced for models of cellular processes was shown in [6].

A system is called robust to a specific class of perturbations if it can maintain its function or structure under these perturbations [7]. Such perturbations include changes in biochemical parameters (e.g. temperature [8] and other environmental changes), molecular noise [9–12], changes of molecular concentrations, as well as mutations [13,14]. Many properties of biochemical systems show some robustness to such perturbations [15–21]. These observations raise the possibility that robustness itself could be used to discriminate between models [15,16]. In the absence of other criteria, a model would be judged superior if it is more robust than other models to some class of perturbations [19]. This notion forms the cornerstone of our contribution.

Conventional methods used in robustness analysis can be subdivided into global and local methods. Global methods characterize properties of a model's parameter space, such as

Author Summary

Robustness is an intrinsic property of many biological systems. To quantify the robustness of a model that represents such a system, two approaches exist: global methods assess the volume in parameter space that is compliant with the proper functioning of the system; and local methods, in contrast, study the model for a given parameter set and determine its robustness. Local methods are fundamentally biased due to the *a priori* choice of a particular parameter set. Our ‘glocal’ analysis combines the two complementary approaches and provides an objective measure of robustness. We apply this method to two prominent, recent models of the cyanobacterial circadian oscillator. Our results allow discriminating the two models based on this analysis: both global and local measures of robustness favor one of the two models. The ‘glocal’ method also identifies key factors that influence robustness. For instance, we find that in both models the most fragile reactions are the ones that affect the concentration of the feedback component.

the size or volume that generate a behavior of interest [22,23], or a parameter’s bifurcation diagram [24–26]. Such a diagram characterizes how qualitative model properties, such as stability of steady-states, change as model parameters are varied [27]. The structure of a bifurcation diagram can be influenced by variation in parameters that are not considered, which limits this approach. Finally, multivariate continuation methods [28] do not show a strong advantage over unrestricted sampling for high-dimensional systems, as they reduce the sampling space only by one dimension.

In contrast to global methods, local methods analyze how perturbations affect model behavior for one specific set of parameters. Their main limitation is precisely this: they may not reflect model behavior under all possible parameters sets. Most robustness analyses in the literature are local. Examples include sensitivity analysis [29], which studies the effect of perturbations for a given parameter set on model behavior, and its application to circadian oscillators [17,18,29]. These methods are usually based on the linearization of a system and therefore hold for variations of only a few percent of the parameter values. Other work uses stochastic simulations to estimate the robustness of a system to molecular noise [11,12]. Efforts to extend a local analysis to systematic parameter variations in more than one or two dimensions [25,26] are often limited by computational cost.

We here propose a novel ‘glocal’ method for analysis and quantification of robustness that combines a global with a local approach. Understanding the origin of robustness and fragility may inform new experiments that can best discriminate between competing hypothetical mechanisms or models. Briefly, the global approach aims at estimating the volume in parameter space occupied by parameters for which a model yields a biologically observed behavior. Because such a search becomes very challenging in high-dimensional parameter spaces, we guide this search through an iterative procedure that involves principal component analysis (PCA) [30]. The second, local aspect of our method evaluates the robustness of model behavior – for each of the previously generated parameter sets – to five different kinds of perturbations, including concentration perturbations and molecular noise. Conceptually our method is different from parameter fitting in the sense that it provides the parameter region where the model is consistent with experimental observations instead of a single parameter set.

To illustrate the application of our method, we focus on two recent models of the cyanobacterial circadian oscillator [31,32]. Circadian

oscillators drive activity patterns of a 24 hour period in many animals, most plants [33], and some bacteria [34]. In cyanobacteria, the purpose of this oscillator is to regulate gene expression, mainly in order to alternate between the exclusive processes of nitrogen fixation and photosynthesis according to light availability [34]. Experiments with mutants have shown that cyanobacteria with a too short- or long-period are eliminated under selection pressure against wild-type organisms synchronized with the 24-hours light/dark cycle [35]. The cyanobacterial oscillator has been reconstituted *in vitro* [36], and is one of the simplest known in any organism [34]. It involves three main proteins called KaiA, KaiB and KaiC. When mixed with ATP, reaction buffer and appropriate concentrations of KaiA and KaiB, KaiC continuously oscillates between a low phosphorylated state and a high one [36]. KaiA and KaiB modulate the phosphorylation status of KaiC. Specifically, KaiA catalyzes KaiC phosphorylation and also seems to inhibit its dephosphorylation. KaiB antagonizes the action of KaiA when KaiC is highly phosphorylated [37]. Highly phosphorylated KaiC is likely to be the readout component because it can bind DNA [38] and thus regulate the expression of other genes. *In vivo*, additional proteins interact with the three core proteins to entrain the cycle and communicate the output signal to the cell. We here focus on models that involve the three core proteins, because these are necessary and sufficient for autonomous oscillations.

We chose this study system for several reasons. First, it is an area of very active recent model development, [31,32,37,39,40], driven by recent insights into the molecular mechanisms of the oscillator [36]. Second, the behavior or function of circadian oscillators is well-characterized: an ample oscillation with a period of approximately 24 hours [34], and low sensitivity to non-periodic environmental perturbations. Third, *in vitro* and *in vivo* experiments show that the cyanobacterial circadian clock is robust to many perturbations [41,42]. Fourth, good estimates for the *in vivo* abundance of all involved proteins and of the cell volume for the cyanobacteria are available. Finally, being posttranslational, the clock shares many features with signal transduction pathways, an important field of application for robustness analysis [43,44]. In order to relate our work to previous robustness studies on transcriptional circadian oscillators [1,2,45,46] we also characterize a prototypical such oscillator in the supplementary material (see Text S1, section C).

Results

‘Glocal’ Robustness

A model’s behavior is determined by some number p of parameters, i.e., the *parameter vector* \mathbf{k} . Any robustness analysis needs to quantitatively characterize the system’s function that is maintained under perturbations. We do this through a collection of *systemic properties* $\boldsymbol{\pi}(\mathbf{k})$ that are required to assume values within predetermined intervals. In our application $\boldsymbol{\pi}$ comprises the period π_T and amplitude π_A of the circadian oscillation of phosphorylated KaiC. We say the oscillator with parameter vector \mathbf{k} maintains its function and *preserves* $\boldsymbol{\pi}$ if $\boldsymbol{\pi}(\mathbf{k}) \in [\boldsymbol{\pi}, \bar{\boldsymbol{\pi}}]$, where we chose these bounds [35] to be 10% below and above published values [31,32]. In the following passages, however, we refer to some general and hypothetical vector of properties $\boldsymbol{\pi}$ to emphasize the generality of our approach.

The first step of our approach involves the sampling of a large set \mathcal{S} of vectors \mathbf{k} that span several orders of magnitude for each component. Only a subset $\mathcal{V} \subset \mathcal{S}$ will generally preserve $\boldsymbol{\pi}$. We call such parameter vectors *viable*. We sample according to an iterative scheme, where in each step the sampling distribution is adjusted based on a PCA of the viable set of the previous step (Figure 1A). After a Monte Carlo integration (Figure 1B), the volume occupied by the set \mathcal{V} provides a first, crude characterization of a model’s

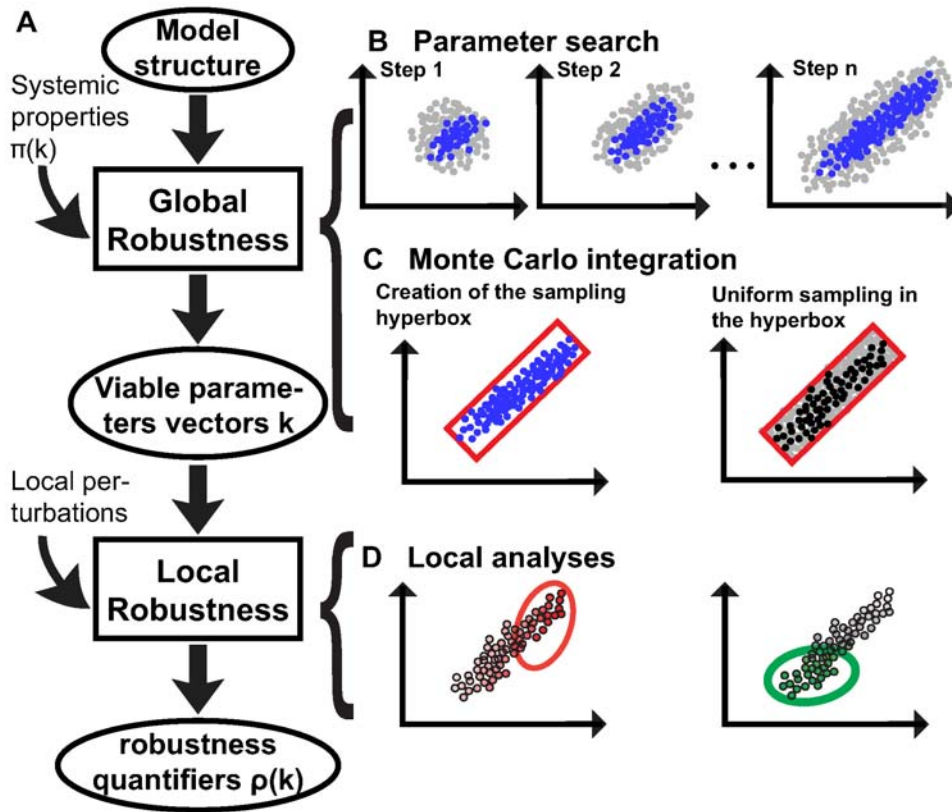


Figure 1. Glocal robustness analysis flow for a hypothetical two dimensional parameter space. (A) A model structure and systemic properties serve as inputs for the global step of the analysis. This global analysis is composed of (B) and (C) and yields viable parameter vectors \mathbf{k} for the model in addition to the normalized viable volume R . Different local perturbations are applied to these parameter vectors (D) in order to quantify their local robustness $\rho(\mathbf{k})$. (B) Monte Carlo sampling to define viable parameter ranges. The first sampling step uses Gaussian random sampling with independently and identically distributed random variables. Some of the tested parameter vectors (gray circles) are viable (blue circles). For subsequent iterative steps, sampling occurs according to the covariance matrix of viable parameters estimated in previous steps. (C) Monte Carlo integration. To estimate the volume in which viable parameter sets occur, we define a hyperbox (red rectangle in left panel) that contains all the viable parameters of the last iteration. We then sample uniformly parameter vectors from this box (right panel, gray circles) and estimate the fraction of viable parameter vectors (right panel, black circles). (D) Local analyses are performed on all viable parameter vectors and help identify correlations between parameter vectors or their components, and robustness values (color intensity) to provide regions of high robustness in the parameters space; two different local robustness quantifiers (left-red, and right-green). doi:10.1371/journal.pcbi.1000534.g001

robustness and can aid in model discrimination by proper normalization. Unless otherwise mentioned, all calculations and observations below are made in the decadic logarithmic domain, because of the broad ranges of parameter values we explore.

The next step of our approach takes advantage of *all* previously identified viable parameter vectors in order to carry out a local robustness analysis. (Figure 1C). This is done by defining a vector of robustness quantifiers $\rho(\mathbf{k})$ for each $\mathbf{k} \in \mathcal{V}$. Specifically, we use five complementary quantifiers to assess the robustness of model properties π to particular kinds of perturbations. We normalize the local robustness quantifiers to range from zero (minimal robustness) to one (maximal robustness). Because the set \mathcal{V} consists of a finite number of sampled parameter vectors, we use statistical tests to assess the results of our analyses. In *Methods* we provide details on the iterative sampling scheme, the volume occupied by \mathcal{V} , and the five local robustness quantifiers.

Two oscillator models

We now apply our approach to two recently proposed mathematical models of the cyanobacterial circadian oscillator. As briefly discussed above, this oscillator involves three core

proteins, KaiA, KaiB, and KaiC, which form complexes with one another (denoted as KaiAB, KaiABC, etc.).

The first model [31] (Figure 2A, see Text S1, section A.4, for equations) involves complex formation of KaiC with the other proteins, as well as cyclic phosphorylation and dephosphorylation of KaiC. In this model, KaiA first binds to KaiC (top reaction of Figure 2A). The resulting complex KaiAC catalyzes the phosphorylation of KaiC forming KaiAC*. A central element of this model is that KaiAC* then exerts a positive feedback on its own formation (red arrow in Figure 2A). In a subsequent step, KaiB binds to the complex KaiAC* and inhibits this autocatalysis. To complete the cycle, KaiA is released, followed by KaiB, and KaiC* is dephosphorylated. We will refer to this model as the *autocatalytic* model.

The second model [32] (Figure 2B, equations in Text S1, section A.5) takes into account two sites S and T of phosphorylation for KaiC [47], resulting in three possible phosphorylated states: KaiC^T, KaiC^S and KaiCST. KaiA catalyzes the phosphorylation of KaiC, KaiC^T and KaiC^S and inhibits the dephosphorylation of KaiCST and KaiC^S. These actions of KaiA are inhibited by KaiC^S (red bar in Figure 2B). Although KaiC^S exerts its effects on KaiA jointly with KaiB [48], KaiB does not

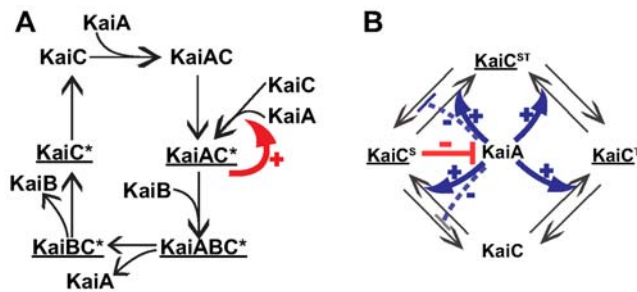


Figure 2. Two models of the cyanobacterial circadian cycle. (A) Autocatalytic model from Mehra et al. [31]. ‘C*’ stands for phosphorylated KaiC. The cycle proceeds clockwise, starting from the upper left. The sum of concentrations of the KaiC*-containing complexes (underlined) form the output of the model. The red arrow denotes the autocatalytic effect of KaiAC* on its synthesis. (B) Two phosphorylation sites model from Rust et al. [32]. There are three possible phosphorylated states for KaiC: KaiC^T, KaiC^S and KaiCST. The sum of concentrations of phosphorylated KaiC molecules (underlined) is the output of the system. KaiA catalyzes phosphorylation reactions (solid blue arrows) and inhibits some dephosphorylation reactions (dashed blue bars). KaiC^S (complexed with KaiB, not explicitly modeled) inhibits the action of KaiA (red bar). doi:10.1371/journal.pcbi.1000534.g002

appear in the equations, because it is assumed to be at saturation level in this model. We will refer to this model as the *two (phosphorylation) sites* model.

Both models capture important empirical observations about the cyanobacterial circadian cycle: phosphorylation of KaiC with the help of KaiA [47], inhibition of this effect by KaiB when bound to phosphorylated KaiC [47–49], and finally dephosphorylation to complete the cycle [47]. However, the models are also fundamentally different in some key assumptions about the underlying mechanism. Because of these dramatic differences, biochemical data will play a decisive role in model discrimination. The robustness analysis we carry out is a first step towards such validation.

The two-sites model shows greater global robustness

In applying our global approach to both models, we sampled parameter vectors covering an enormous range of six orders of magnitude for each parameter, centered on published [31,32]

parameter values for both models (see *Methods* and Text S1, sections A.4 and A.5, for parameter values). We carried out our procedure for ten PCA iterations and used the viable parameters of the last four iterations to define the hyperbox for the Monte Carlo integration.

Figure 3A shows the (normalized) viable volumes R for the two models. These volumes can be interpreted as the average allowable variation per parameter that leaves the circadian oscillations intact. The two-sites model is vastly more robust than the autocatalytic model. Specifically, the value $R=0.718$ for the autocatalytic model means that the parameters can vary over 0.7 orders of magnitude, or 5.2-fold. For the two-sites model, the value of $R=1.60$ is more than twice that, correspond to a 39-fold allowable variation. The values shown are based on at least 5×10^4 parameter vectors and have sampling errors of less than one percent (see *Methods* for details). We also note that the estimated viable parameter volumes were highly reproducible among five independent applications of the iterative procedure. For example, the mean values of $R=1.60 \pm 0.01$ (two-sites model) and $R=0.718 \pm 0.006$ (autocatalytic model) have a coefficient of variation below one percent over these five iterations, which shows that the PCA-guided sampling approach gives highly reproducible results.

What is responsible for the lower robustness of the autocatalytic model? One possibility is that strong associations exist between individual parameters in viable parameter sets, such that some parameters cannot vary independently from others. Such associations, if present, may also provide mechanistic insights into complex, high-dimensional circuits. Figure 3B shows the standard deviations of viable parameters along the principal axes of both models. With one exception, the amount of variation along most principal component axes is similar for both models. The exception (indicated by the arrow in the Figure 3B) is the lowest PCA axis for the autocatalytic model.

The high constraint on variation in this axis is caused by a strong positive correlation between the rate for the autocatalytic reaction, parameter k_3 , and the rate for the formation of the complex KaiABC*, k_4 (Figure 3C). This axis deviates by merely 13 degrees from the vector $\mathbf{k}=(0,0,1,-1,0,0,0)$ defined by these parameters. Parameters k_3 and k_4 are highly correlated (Pearson’s $r=0.97$, significance of all statistical tests are summarized in Table 1). This strong association contributes to the lack of global robustness we observe in the autocatalytic model. It means that a

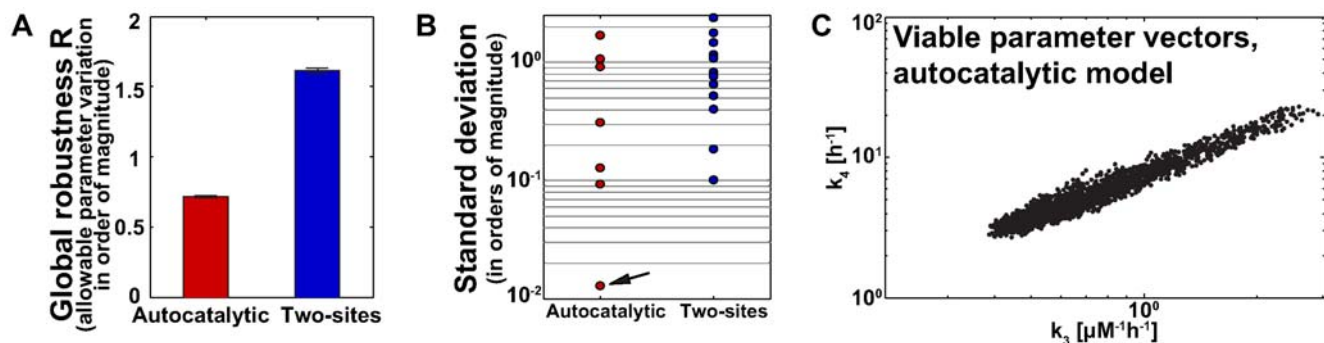


Figure 3. Results of the global robustness analyses for both models. (A) The two-sites model (right) has significantly greater normalized viable volume than the autocatalytic model (left). Error bars (<1%) correspond to standard deviations over five independent estimates. (B) Standard deviations along the principal axes of viable parameters for the autocatalytic model and the two-sites model. Note the logarithmic scale. The autocatalytic model has a strongly constrained axis (arrow); amounts of variation along the other axes are overall smaller for the autocatalytic model. (C) Projection of the viable vectors of the autocatalytic model after the MC integration on the plane (k_3, k_4). These two parameters are strongly correlated resulting in the lowest standard deviation for the autocatalytic model (B). doi:10.1371/journal.pcbi.1000534.g003

Table 1. Statistical tests and their significance used to assess model discrimination and correlations.

Null hypothesis	Test type	r-value	p-value	n
Parameters k_3 and k_4 are correlated in the autocatalytic model	Pearson's	0.97	$<10^{-323}$	1828
ρ_P is larger for two-sites model	Wilcoxon rank		3.32×10^{-91}	
ρ_P correlated with k_7 for autocatalytic model	Spearman's	-0.638	$<10^{-323}$	1828
robustness to temperature changes is larger than ρ_P for autocatalytic model	Wilcoxon rank sum		1.95×10^{-246}	
robustness to temperature changes is larger than ρ_P for two-sites model	Wilcoxon rank sum		0.245	
robustness to temperature changes is larger for two-sites model	Wilcoxon rank sum		2.28×10^{-4}	
ρ_C is larger for two-sites model	Wilcoxon rank		9.25×10^{-177}	
ρ_P correlated with k_7 for autocatalytic model	Spearman's	-0.718	2.81×10^{-289}	1828
ρ_N is larger for two-sites model	Wilcoxon rank		3.09×10^{-239}	
ρ_A is larger for two-sites model	Wilcoxon rank		4.31×10^{-10}	
ρ_S is larger for two-sites model	Wilcoxon rank		1.69×10^{-151}	
ρ_T is larger for two-sites model	Wilcoxon rank		1.48×10^{-238}	
ρ_T is correlated with the distance from the parameter with the highest ρ_T for autocatalytic model	Spearman's	-0.355	$<10^{-323}$	1828
ρ_T is correlated with the distance from the parameter with the highest ρ_T for two-sites model	Spearman's	-0.196	$<1.15 \times 10^{-6}$	604

doi:10.1371/journal.pcbi.1000534.t001

perturbation of parameter k_3 that would not be followed by a corresponding perturbation in parameter k_4 would prevent the model to preserve properties π of interest. When we examine the structure of the equations for the autocatalytic model (Figure 2A), we find that the mechanistic cause for this association lies in the dynamics of KaiAC*: on the one hand, if k_3 is too large, the concentration of KaiAC* increases too fast and the autocatalytic effect is too strong; on the other hand, if k_4 is too large, the concentration of KaiAC* is too low and the autocatalytic effect is too weak. The parameters k_3 and k_4 need to be delicately balanced to have the correct concentration of KaiAC* resulting in the appropriate feedback strength.

To assess whether this strong association is responsible for the smaller global robustness of the autocatalytic model, we collapsed the highly correlated parameters k_3 and k_4 into one. That is, we assumed that k_3 and k_4 are linearly dependent and can be considered as one single parameter. The reduced model with only six parameters yields a global robustness estimate of $R = 1.09$. This corresponds to an allowable 12-fold average variation of each parameter, and accounts partially for the lower robustness of the autocatalytic model.

A remaining question is whether the viable region of parameter space forms a connected set. Such connectedness would facilitate the evolution of oscillators with high robustness through gradual changes of individual parameters. Although this question cannot be answered rigorously by our sampling approach we show that this is probably the case for both models (Text S1, section B.1, and Figure S1).

The two-sites model shows greater overall local robustness

Figure 4A shows the distribution of ρ_P , our quantifier of robustness to local parametric perturbations for both the autocatalytic model and the two-sites model. The median robustness of the autocatalytic model is lower by 29% (median $\rho_P = 0.179$ and $\rho_P = 0.231$ for the autocatalytic and two-sites model, respectively; see table 1 for significance).

Our combination of global and local analysis allows us to ask whether individual chemical reactions (represented through their

parameters) are particularly important for a model's robustness. To this end, we investigated whether there exist statistical associations between ρ_P and any of the model parameters. One striking such association stands out for the autocatalytic model (Figure S2A). Specifically, ρ_P is highly associated with k_7 , (Spearman's $r = -0.638$), whereas all other parameters and ρ_P show only $r < 0.11$ (Spearman's partial correlation given k_7). A glance at the model equations (Text S1, section A.4) shows that the reaction associated with k_7 dephosphorylates KaiC* and thus triggers the initialization of a new autocatalytic cycle. If this initialization occurs too fast (at large k_7), synchronization of complex formation and absorption of perturbations is poor.

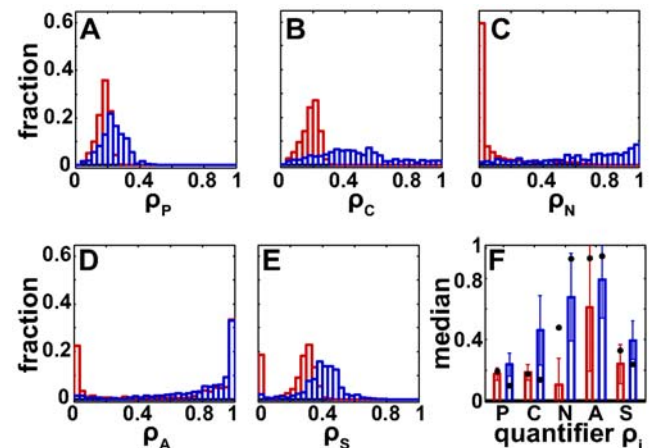


Figure 4. The two-sites model (blue) has greater local robustness than the autocatalytic model (red). Shown are the distributions of (A) robustness to local parameter perturbations ρ_P , (B) robustness to total concentration perturbations ρ_C , (C) robustness to molecular noise ρ_N , (D) attraction of the cycle ρ_A , and (E) sensitivity of the period ρ_S . In (F) median values are shown with their associated standard deviation (error bars) for both models and all five quantifiers. Black dots indicate local robustness values for the previously published parameter vector's [31,32].

doi:10.1371/journal.pcbi.1000534.g004

As an extension of this quantifier, properly correlated parametric perturbations are used to address the robustness to temperature changes (see *Methods*). We find that the two-sites model has a median robustness only 4% greater than the autocatalytic model (Figure S3B). Individual analyses of both models show why this difference, yet significant ($p=2.28 \times 10^{-4}$), is small compared to the difference in ρ_P . On the first hand, the autocatalytic model is more robust to such correlated perturbations than to uncorrelated perturbations (median of 0.230, and 0.179, respectively). The large difference between the two cases for the autocatalytic model (Figure S3A and S3B, red bars) can be explained by the strong association between k_3 and k_4 discussed above: correlated perturbations cannot be aligned with the most constrained direction of the viable parameter volume. On the other hand, the two-sites model, which does not have such highly associated parameters, does not show increased robustness to correlated parameter changes ($p=0.245$).

We next turn to total concentration perturbations ρ_C (distribution shown in Figure 4B). Here, the two-sites model is on average 2.5-fold more robust than the autocatalytic model, with a median $\rho_C=0.192$ and $\rho_C=0.439$ for the autocatalytic and two-sites model, respectively. For instance, for 10% of viable parameter vectors in the two-sites model, more than 80% of perturbations leave the circadian oscillation intact. Exactly as for ρ_P , we find that in the autocatalytic model, k_7 strongly influences ρ_C (Figure S2B), with a Spearman's rank correlation between k_7 and ρ_C of -0.718 , which underscores the importance of this dephosphorylation reaction.

We next assessed robustness ρ_N to molecular noise. To this end, we used Gillespie's algorithm [50] to simulate an oscillator with 2000–6000 molecules in a reaction volume of $3\mu\text{L}$, numbers that are of the correct order of magnitude for the number of Kai proteins in a cyanobacterial cell [49]. Here again, the two-sites model is significantly more robust, with a median (mean) value of ρ_N that is 45 (6.5) times larger (Figures 4C and 4F). For example, for the autocatalytic model, fewer than 6% of viable parameter vectors show $\rho_N > 0.5$ (Figure S2C), whereas more than 80% of the parameters show $\rho_N > 0.5$ in two-sites model, where noise also affects only a small region of the viable parameter volume (Figure S2D). We discuss in the Text S1, sections B.3 and B.4, that the reactions forming KaiAC, and those forming and destroying KaiC^S are of particular importance for robustness to molecular noise.

We next turn to the attraction of the cycle ρ_A , whose distribution is shown in Figure 4D. The two-sites model has a significantly higher median $\rho_A=0.891$ compare to $\rho_A=0.846$ for the autocatalytic model. An analogous difference holds for period sensitivity (Figure 4E), where ρ_S is on average 65 percent greater in the two-sites model.

We had noted previously that k_3 and k_4 are strongly and negatively associated with global robustness. When analyzing their association with period sensitivity, we find that they also have a strong and opposite impact on the period (results not shown). The reason is the same as discussed in the results for global robustness, namely that the autocatalytic feature that is so central to this model requires a delicate balance of two reactions producing and destroying KaiAC*. This feature also explains the higher robustness to temperature compensation as discussed above.

To summarize, the two-sites model shows significantly greater values in each of the local robustness quantifiers we used (Figure 4F). It is thus not surprising that the average ρ_T of all five quantifiers also indicates much greater robustness for the two-sites model. For this model, robustness also decreases more slowly with distance from the points of highest average local robustness

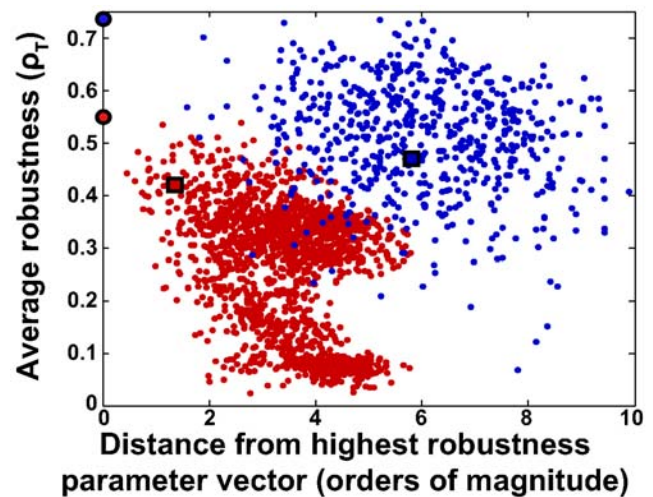


Figure 5. Distribution of the average local robustness ρ_T for the two models. For each viable parameter vector \mathbf{k} , the figure shows its distance (horizontal axis) from the viable parameter vector with the highest average local robustness ρ_T plotted against the ρ_T of \mathbf{k} (vertical axis); autocatalytic model (red) and two-sites model (blue). Large circles correspond to the two parameter vectors with the highest ρ_T for each model, and squares correspond to published parameter vectors [31,32]. The greater the distance of \mathbf{k} to the most robust parameter vector, the lower its ρ_T . This negative association is stronger for the autocatalytic model.

doi:10.1371/journal.pcbi.1000534.g005

reflecting a larger volume with high average robustness (Figure 5; see Text S1, section B.5 for details).

Discussion

Most published work on the robustness of cellular circuits addresses either global or local robustness [17,18,20,29]. Our ‘glocal’ approach overcomes the limitations of both global and local analyses. First, by generating large samples of parameter vectors, the approach can estimate a viable volume of parameter space that yields a behavior of interest. It is thus not easily misled by results derived from a particular chosen point in parameter space, in contrast to parameter fitting that yields only single point estimate. This feature is particularly important for biochemical models that are *structurally* or *practically* unidentifiable [5,6,51,52]. For the potentially large class of models with this property, model parameters that yield an observed behavior cannot be uniquely identified even in the presence of arbitrarily abundant and error free data. In order to discriminate between possible parameters and models, new experiments could be designed using the results of our robustness analysis. Second, the analysis of parameter vectors spanning multiple orders of magnitude shows how local robustness varies in parameter space. Third, a combination of local and global analyses lends itself to deeper mechanistic insight into circuit behavior. In particular, it can lead to the identification of key parameters important for robustness. Obvious applications include synthetic biology, where tunability of a synthetic circuit's robustness by changing key parameters is highly desirable. Finally, by studying different quantifiers of local robustness, one can obtain trade-offs between robustness and other system properties.

Methods similar to the global part of our approach have been proposed earlier [22,53]. However, by using principal component analysis, our global method samples more efficiently, a necessity for studying high dimensional parameter spaces.

Potential limitations of our approach include the requirement for a starting parameter vector to initialize global sampling. We used published information for this vector [31,32]. However, even where such information is unavailable, random sampling and optimization techniques [4] are available to permit creation of such a vector. A second limitation regards the range of the region in parameter space from which one samples. To avoid biased estimation of robustness, the size of this range should be chosen beyond the biophysical bounds on parameters. Note that a conservative choice of this range does not hamper our approach, because our iterative procedure quickly directs the sampling to viable regions.

A third potential limitation regards computational requirements, because our global approach requires numerical integration of a model for hundreds of thousands of parameter vectors, and local robustness estimation for thousands of these vectors. Nonetheless, the approach is feasible with currently available technology. For example, global robustness analysis for the 12-dimensional two-sites model involving nearly 10^6 parameter vectors, and 10^3 local perturbations for each of the resulting viable vectors executes in less than 5 days on a commercially available eight-core (Intel Xenon X5355 @ 2.66 GHz) architecture. The inevitable exponential scaling of complexity with parameter dimensions can only be mitigated by a guided sampling procedure like ours.

In our application of the method to two circadian oscillator models, we find that the two-sites model shows vastly greater global robustness than the autocatalytic model, with 39-fold and 5-fold allowable parameter variation, respectively, along each parameter dimension on average. Similarly, the two-sites model is also more robust for each of several different quantifiers of local robustness, including robustness to parameter changes, molecular noise, transient state perturbation, and period sensitivity. Based on these considerations alone, the architecture of the two-sites model is superior to the one of the autocatalytic model. If robustness is advantageous, and if this oscillatory mechanism is realizable biochemically [35,41], it should be the preferred architecture. This observation is consistent with recent experiments that provide strong evidence in favor of ordered phosphorylation in the cyanobacterial clock [47,54]. In contrast, the autocatalytic mechanism [31], obtained by interpreting experimental results of [49], whereas phosphorylated KaiC facilitates KaiA-KaiC association and subsequent KaiC phosphorylation, was not confirmed by recent experiments [32,47,54].

The ‘glocal’ combination of global and local robustness analysis shows which chemical reactions in these models are of particular importance for robustness (or a lack thereof). For example, the rates of two central reactions of the autocatalytic loop in the autocatalytic model need to be delicately balanced, a property that partially accounts for its lack of global robustness. Put differently, the central feature of this model is partly responsible for its low robustness. In the two-sites model, our local analysis shows that the rates of the reactions that form and destroy KaiC^S are of particular importance for its robustness. For low values of these parameters, the concentration of KaiC^S fluctuates to a greater extent. The resulting fluctuations are then amplified by the feedback loop central to this model. In addition to the analysis of these two cyanobacterial circadian models, results obtained with the Goodwin model (see Text S1, section C) show the feasibility of this glocal method for models with a different structure. Our analysis of this generic circadian oscillator also demonstrates the importance of a tight regulation of the feedback component.

In both cyanobacterial models, our evidence suggests that the regions of parameter space where viable parameters occur are

connected. This observation is significant to understand how robustness of circadian oscillations could evolve [52,55,56], in particular through gradual, small changes of individual parameters. The volume formed by these parameter vectors likely forms a ‘neutral volume’ [57] in which circadian oscillations with a given period and amplitude are preserved. However, what is changing in this volume is local robustness. Thus, if local robustness (or one aspect thereof) is adaptive, then robust circuits are readily accessible to natural selection through the connectedness of the neutral volume, without the need to change the oscillatory behavior itself. In this regard, it is also intriguing to see that the published parameter vectors for either model do not show maximal robustness. If these vectors reflect biological reality, then optimization criteria aside from robustness remain to be discovered, or some unknown constraint may prevent maximization of robustness.

Methods

The first, global part of our method identifies the viable set \mathcal{V} for a given sampled set \mathcal{S} that comprises of the order of 10^5 parameter vectors uniformly sampled in some closed region of p -dimensional space. We chose the region to be a hyper-cube centered around nominal published values [31,32], spanning six orders of magnitude for each component. In order to avoid biased estimates the interval bounds should be beyond what is biophysical feasible. Such an a priori range needs to be established, both for practical reasons, and for models that are unidentifiable [5,51,52] (see Text S1, section A.1, and Figure S4). The sampling method involves an iterative procedure, which we now describe. In each iterative step j it generates a set $\mathcal{S}^{(j)}$, and identifies the viable subset $\mathcal{V}^{(j)}$. The first set $\mathcal{S}^{(1)}$ is a Monte Carlo sample of the parameter space obtained via a large ($>10^4$) number of p -dimensional Gaussian random variates, centered on a known viable parameter vector [31,32]. (Figure 1A). We then determine the viable subset $\mathcal{V}^{(1)}$ of $\mathcal{S}^{(1)}$, which comprises of the order of 100–1000 elements in our application. The next step of the procedure consists of a principal component analysis (PCA) of the viable parameter set $\mathcal{V}^{(1)}$. PCA is a technique to identify linear statistical structure in high-dimensional data sets [30]. We use it here to identify associations among viable parameters that can guide our sampling in subsequent iterations. Specifically, the set $\mathcal{S}^{(2)}$ and subsequent sets are generated from previous parameter sets as follows

$$\mathcal{S}^{(j)} = \{ \mathbf{k}_i = \langle \mathcal{V}^{(j-1)} \rangle + \lambda^{(j-1)} \boldsymbol{\xi}_i \mid i = 1, \dots, L \}, \quad (1)$$

for all $j > 1$, where $\langle \mathcal{V}^{(j-1)} \rangle$ stands for the element-wise mean of parameter vectors in the set $\mathcal{V}^{(j-1)}$ and $\boldsymbol{\xi}_i$ is the i -th realization of a p -dimensional Gaussian process with zero mean and covariance matrix $\Sigma^{(j-1)}$. The size of $\mathcal{S}^{(j)}$ is given by L ($L = 5 \times 10^4$ in our application). The entries $\Sigma_{nm}^{(j-1)}$ are the pairwise covariances of parameters k_n and k_m in the set $\mathcal{V}^{(j-1)}$. We compute this matrix, whose eigenvectors are the principal axes of the set $\mathcal{V}^{(j-1)}$, through PCA. The real valued factor $\lambda^{(j-1)}$ determines the variance of the j -th Gaussian process by scaling the standard deviations of the distribution along the PCA directions of the $(j-1)$ -th iteration (Figure 1A). In this approach PCA avoids “wasting” sampling effort on parameter regions where viable parameter vectors are not likely to be found. As described thus far, our procedure serves to identify major axes of viable parameter variation for sampling and the dispersion of the viable parameters along them. To establish global measures of robustness, we then perform a Monte Carlo integration (Figure 1B). Specifically, we construct a hyper-

box \mathcal{B} in parameter space whose axes are parallel to the PCA axes of the last iteration. In each dimension, the limits of this box are defined by the most extreme components of the viable parameters found in the last iteration of sampling along these axes. We then generate a set \mathcal{S} of at least 10^5 parameter vectors sampled uniformly within \mathcal{B} , of which some fraction $|\mathcal{V}|$ will be viable. An appropriate global measure of robustness for any one model is the *viable volume* $V = (|\mathcal{V}|/|\mathcal{S}|)(\text{Vol}(\mathcal{B}))$, where $|\cdot|$ denotes the number of elements in a set. The rationale behind this measure is that with increasing robustness V , a perturbation of a parameter or parameter vector is increasingly likely to generate another viable parameter vector. To compare models with different number of parameters, we define the normalized viable volume as robustness $R = \sqrt[p]{V}$. Note that it would not be appropriate to just consider the ratio $|\mathcal{V}|/|\mathcal{S}|$ as a robustness measure when comparing models (Figure S5). The main functions for this analysis, written in MATLAB, are available for download at <http://www.bioc.uzh.ch/wagner/publications-software.html>.

To estimate the sampling errors in the viable fractions and volumes, we note that $|\mathcal{V}|$, as estimated by Monte Carlo integration is a binomially distributed random variable [30,58]. An estimate of its standard deviation is $\sqrt{\frac{|\mathcal{V}|(|\mathcal{S}|-|\mathcal{V}|)}{|\mathcal{S}|}}$. Of interest is the coefficient of variation or relative error, defined as the standard deviation divided by the mean. For $|\mathcal{V}|$, this relative error is given by $\sqrt{\frac{|\mathcal{S}|-|\mathcal{V}|}{|\mathcal{V}||\mathcal{S}|}}$. For the normalized quantity $R = \sqrt[p]{V}$, the relative error needs to be divided by p , i.e., it calculates as

$$\frac{\Delta R}{R} = \left(\frac{1}{p}\right) \sqrt{\frac{|\mathcal{S}|-|\mathcal{V}|}{|\mathcal{V}||\mathcal{S}|}}$$

which scales as $\left(\frac{1}{p}\right) \frac{1}{\sqrt{|\mathcal{S}|}}$. Furthermore we estimate the necessary sample size $|\mathcal{S}|$ for a given relative accuracy δ and confidence. Applying Hoeffding's inequality [59], and exploiting the fact the random variables are binomially distributed, we obtain

$$\Pr\left\{1 - \frac{E(|\mathcal{V}|)}{|\mathcal{V}|} \geq \delta\right\} \leq e^{-2\delta^2 \left(\frac{|\mathcal{V}|}{|\mathcal{S}|}\right)^2 |\mathcal{S}|},$$

where $E(\cdot)$ denotes the expectation operator. Thus, estimating the sampling *acceptance ratio* $|\mathcal{V}|/|\mathcal{S}|$ from a sufficiently large ensemble and assuming it to be constant for the successive sampling, we can compute a lower bound for the necessary sample size. For example, asking for 10% accuracy with a confidence of 95% at an acceptance ratio of 1/20, Hoeffding's bound requires the sample size to be $|\mathcal{S}| > 60000$.

We now briefly comment on how estimation errors scale with the number of dimensions p . The only possible general statement is that the ratio between the viable volume and the volume of the sampling box scale exponentially with p . Therefore, $\frac{|\mathcal{V}|}{|\mathcal{S}|} \sim \alpha^{-p}$ with α being dependent on the geometry of the viable volume. For example, $\alpha = 1$ if the viable volume is identical to the sampling hyper-rectangle, and only in this trivial case does the error not depend on p . If the viable parameter volume has an ellipsoidal shape, and if the dimension increases from $p = 5$ to $p = 22$, then α increases from 1.5 to 2.5. The coefficient of variation (relative error) of the viable volume scales as $\frac{\alpha^{p/2}}{p \sqrt{|\mathcal{S}|}}$. The size and the shape of the sampling hyper-rectangle is crucial for low errors: a larger hyperbox means that an exponentially greater number of points needs to be sampled for high dimensional systems to ensure constant error. These observations underscore the usefulness of PCA, which can dramatically reduce computational requirements.

The second, local part of our method assesses the robustness of every viable parameter \mathbf{k} in terms of five quantifiers. The first local robustness quantifier $\rho_P(\mathbf{k})$ computes to the fraction of local random perturbations of parameters that preserve π . A perturbation is generated by multiplying all parameter values with uncorrelated Gaussian variates of variance $\sigma = 0.2$ and mean 1. To address the robustness to temperature changes the Arrhenius equation has to be used ideally [8,31,46]. However, this approach requires knowledge of the activation energies of each reaction in a system, which is usually not available. We thus simply assume that an increase in temperature corresponds to a random increase of all parameters. This aspect of robustness is quantified with the same approach used for estimating ρ_P . Mean and standard deviation are the same, but perturbations are correlated, such that all parameters are multiplied with variates that are either above one or below one for a particular perturbation. The second local robustness quantifier $\rho_C(\mathbf{k})$ regards alterations in the total amount of key proteins. For example, the *in vitro* reconstitution of the cyanobacterial circadian oscillator uses a pre-determined number of the Kai molecules [37,60]. This number may vary *in vivo*, for example due to changes in cell volume caused by the cell division cycle. To estimate ρ_C , we generate a large number of perturbed concentrations, and numerically integrate the model with these perturbed concentrations. For a given parameter vector $\mathbf{k} \in \mathcal{V}$, we define ρ_C as the fraction of these perturbations preserving π . The third robustness quantifier, $\rho_N(\mathbf{k})$, reflects that chemical reactions are stochastic events [12,20,61]. To quantify robustness to such molecular noise, we perform many stochastic simulations [50], and define for each viable \mathbf{k} , ρ_N as the fraction of trajectories that preserve π . The fourth robustness quantifier, $\rho_A(\mathbf{k})$ (for attraction of the cycle), measures how fast the oscillator returns to its cycling behavior when its trajectory is transiently perturbed with the use of Floquet multipliers. The fifth quantifier, $\rho_S(\mathbf{k})$ (for sensitivity analysis of period), assesses the effect of an infinitesimal change of an individual parameter or parameter vector on the period of a model. The larger the value of ρ_S , the more robust a model is. A value of $\rho_S = 0.5$ means that a one percent change in a parameter vector results in a one percent change in the period. The last two quantifiers are specific to systems involving stable oscillations. For the full mathematical details on these five quantifiers see Text S1, section A.3.

Supporting Information

Figure S1 Viable parameter sets form large connected regions in parameter space. (A) Autocatalytic model, (B) two-sites model. Pairs of viable parameter vectors (black dots) are connected by blue lines, if they are likely to be part of the same connected region of parameter space, as determined by numerical analysis explained in the text. Parameter vectors that cannot be connected to other parameter vectors are shown as red dots. The graph is shown as a projection on to the axes formed by k_5 and k_6 for (A), and as a projection onto the axes formed by k_1 and k_2 in (B), because these projections best illustrate that the viable region is not convex. Found at: doi:10.1371/journal.pcbi.1000534.s001 (0.52 MB PDF)

Figure S2 Correlations of the local robustness quantifiers with model parameter. (A) Parameter k_7 (horizontal axis) negatively affects robustness to parameter perturbations (vertical axis) in the autocatalytic model (Spearman's $r = -0.638$, $p < 10^{-323}$, $n = 1828$). (B) Parameter k_7 (horizontal axis) negatively affects robustness to parameter perturbations (vertical axis) in the autocatalytic model (Spearman's $r = -0.718$, $p = 2.81 \times 10^{-289}$, $n = 1828$). (C) Score for robustness to molecular noise for the autocatalytic model plotted against k_1 and (D) the two-sites models

plotted against k_2 . In the autocatalytic model, k_1 has a Spearman's correlation coefficient with ρ_N of 0.921 ($p < 10^{-323}$, $n = 1828$) and less than 6 percent of the parameter vectors have a score above 0.5. For the two-sites model, k_2 has a correlation coefficient with ρ_N of 0.629 ($p < 10^{-323}$, $n = 604$) and more than 80 percent of the parameter vectors have a score above 0.5.

Found at: doi:10.1371/journal.pcbi.1000534.s002 (0.87 MB PDF)

Figure S3 (A) Distribution of the scores for the robustness to parameter perturbations (autocatalytic model in red and two-sites model in blue), similar as Figure 4B. (B) Distribution of the scores for the robustness to temperature changes. The results are obtained with the same algorithm as the one for ρ_P but the random variates are correlated such that for a particular perturbation all parameters are either increased or decreased. In this case, the median robustness for the two-sites model is only 4 percent larger than the median of the autocatalytic model ($p = 2.28 \times 10^{-4}$, Wilcoxon rank sum test).

Found at: doi:10.1371/journal.pcbi.1000534.s003 (0.09 MB PDF)

Figure S4 Illustration of the proposed sampling approach based on interval constraints. The a priori sampling range (light-gray) and two systemic properties π_1 and π_2 allowed to assume values in predetermined intervals induce constraints in parameter space and partition it into regions that are viable and those that are not. The parameter region preserving π_2 is unbounded, accounting for the situation of unidentifiability and indicates the necessity for an a priori sampling range.

Found at: doi:10.1371/journal.pcbi.1000534.s004 (0.27 MB PDF)

Figure S5 The importance of incorporating volume information in estimating global robustness. One might argue that it would be sufficient to just use the ratio $C = |V|/|S|$ as a measure of global robustness. This is not the case if one wants to compare models where both the geometry and the size of a model's viable set vary

among models. The reason is that the geometry of the viable volume critically influences C . The Figure shows the shape of viable sets and the circumscribed hyperbox for three hypothetical models. The viable sets in (A) and (C) have very different shapes, but fit into a hyperbox of the same size. If these models are compared, the size of the hyperbox would therefore be irrelevant (and one would say that the model of (A) has greater robustness than the model of (B)). The viable sets in (A) and (B) have the same geometry but the viable set of (B) can be circumscribed by a smaller hyperbox. The ratio C would be the same for these two models. The models in (B) and (C) have both a different geometry and extension. In that case the differing box volumes must be taken into account, and the expression $V = (|V|/|S|) \cdot \text{Vol}(B)$ accomplishes that. Put differently, it would be appropriate to use the ratio C only if parameter sets were to be sampled from boxes of the same size for different models, an approach that we avoid, because it would lead to very large errors in the Monte Carlo integration for some models.

Found at: doi:10.1371/journal.pcbi.1000534.s005 (0.31 MB PDF)

Text S1 Supplementary methods, supplementary results, robustness analysis of the Goodwin model and supplementary figures S6 to S11.

Found at: doi:10.1371/journal.pcbi.1000534.s006 (2.41 MB PDF)

Acknowledgments

The authors want to thank the reviewers for their helpful comments.

Author Contributions

Conceived and designed the experiments: MH HK AW. Performed the experiments: MH. Analyzed the data: MH HK AW. Contributed reagents/materials/analysis tools: MH HK MH. Wrote the paper: MH HK AW.

References

- Goldbeter A (1996) *Biochemical Oscillations and Cellular Rhythms*. Cambridge: Cambridge University Press.
- Alon U (2007) *An Introduction to Systems Biology*. Boca Raton, FL: Chapman & Hall/CRC.
- Liebermeister W, Klipp E (2005) Biochemical networks with uncertain parameters. *IEE Proc-Syst Biol* 152: 97–105.
- Moles C, Mendes P, Banga J (2003) Parameter estimation in biochemical pathways: A comparison of global optimization methods. *Genome Research* 13: 2467–2474.
- Hengl S, Kreutz C, Timmer T, Maiwald (2007) Data-based identifiability analysis of non-linear dynamical models. *BMC Bioinformatics* 23: 2612–2618.
- Gutenkunst R, Waterfall J, Casey F, Brown K, Myers C, et al. (2007) Universally sloppy parameter sensitivities in systems biology models. *PLoS Comput Biol* 3: 1871–1878.
- Kitano H (2007) Toward a theory of biological robustness. *Mol Syst Biol* 3: 137.
- Ruoff P (1992) Introducing temperature-compensation in any reaction kinetic oscillator model. *J Interdiscipl Cycle Res* 23: 92–99.
- McAdams HH, Arkin A (1997) Stochastic mechanisms in gene expression. *Proc Natl Acad Sci USA* 94: 841–819.
- Swain PS, Elowitz MB, Siggia ED (2002) Intrinsic and extrinsic contributions to stochasticity in gene expression. *Proc Natl Acad Sci USA* 99: 12795–12800.
- Gonze D, Halloy J, Goldbeter A (2002) Robustness of circadian rhythms with respect to molecular noise. *Proc Natl Acad Sci USA* 99: 673–678.
- Gonze D, Goldbeter A (2006) Circadian rhythms and molecular noise. *Chaos* 16: 026110.
- Nowak MA, Boerlijst MC, Cooke J, Smith JM (1997) Evolution of genetic redundancy. *Nature* 388: 167–171.
- Wagner A (2000) Robustness against mutations in genetic networks of yeast. *Nat Genet* 24: 355–361.
- Morohashi M, Winn AE, Borisuk MT, Bolouri H, Doyle J, et al. (2002) Robustness as a measure of plausibility in models of biochemical networks. *J Theor Biol* 216: 19–30.
- Stelling J, Sauer U, Szallasi Z, Doyle FJ III, Doyle J (2004) Robustness of cellular functions. *Cell* 118: 675–685.
- Stelling J, Gilles ED, Doyle FJ III (2004) Robustness properties of circadian clock architectures. *Proc Natl Acad Sci USA* 101: 13210–13215.
- Rand DA, Shulgin BV, Salazar JD, Millar AJ (2006) Uncovering the design principles of circadian clocks: Mathematical analysis of flexibility and evolutionary goals. *J Theor Biol* 238: 616–635.
- Wolf J, Becker-Weimann S, RH (2005) Analysing the robustness of cellular rhythms. *Syst Biol* 2: 35–41.
- El-Samad H, Kurata H, Doyle J, Gross CA, Khammash M (2005) Surviving heat shock: Control strategies for robustness and performance. *Proc Natl Acad Sci USA* 102: 2736–2741.
- Doyle J, Csete M (2005) Motifs, control, and stability. *PLoS Biol* 3: 1868–1872.
- Eissing T, Allgöwer F, Bullinger E (2005) Robustness properties of apoptosis models with respect to parameter variations and intrinsic noise. *IEE Proc-Syst Biol* 152: 221–228.
- Dayarian A, Chaves M, Sontag E, Sengupta A (2009) Shape, size, and robustness: Feasible regions in the parameter space of biochemical networks. *PLoS Comput Biol* 5: 1–12.
- Ma L, Iglesias PA (2002) Quantifying robustness of biochemical network models. *BMC Bioinformatics* 3.
- Battotokh D, Tyson JJ (2004) Bifurcation analysis of a model of the budding yeast cell cycle. *Chaos* 14: 653–661.
- Leloup JC, Goldbeter A (2004) Modeling the mammalian circadian clock: Sensitivity analysis and multiplicity of oscillatory mechanisms. *J Theor Biol* 230: 541–562.
- Steuer R, Gross T, Selbig J, Blasius B (2006) Structural kinetic modeling of metabolic networks. *Proc Natl Acad Sci USA* 103: 11868–118734.
- Henderson ME (2002) Multiple parameter continuation: computing implicitly defined k-manifolds. *Int J Bifurcation Chaos* 13: 451–476.
- Bagheri N, Stelling J, Doyle FJ III (2007) Quantitative performance metrics for robustness in circadian rhythms. *Bioinformatics* 23: 358–364.
- Fukunaga K (1990) *Introduction to Statistical Pattern Recognition*. San Diego: Academic Press, 2nd edition.
- Mehra A, Hong CI, Shi M, Loros JJ, Dunlap JC, et al. (2006) Circadian rhythmicity by autocatalysis. *PLoS Comput Biol* 2: 816–823.
- Rust MJ, Markson JS, Lane WS, Fisher DS, O'Shea EK (2007) Ordered phosphorylation governs oscillation of a three-protein circadian clock. *Science* 318: 809–812.
- Doyle FJ III, Gunawan R, Bagheri N, Mirsky H, To TL (2006) Circadian rhythm: A natural, robust, multi-scale control system. *Comput Chem Eng* 30: 1700–1711.

34. Ditty JL, Williams SB, Golden SS (2003) A cyanobacterial circadian timing mechanism. *Annu Rev Genet* 37: 513–543.
35. Ouyang Y, Andersson CR, Kondo T, Golden SS, Johnson CH (1998) Resonating circadian clocks enhance fitness in cyanobacteria. *Proc Natl Acad Sci USA* 95: 8660–8664.
36. Nakajima M, Imai K, Ito H, Nishiwaki T, Murayama Y, et al. (2005) Reconstitution of circadian oscillation of cyanobacterial KaiC phosphorylation in vitro. *Science* 308: 414–415.
37. Mori T, Williams DR, Bryne MO, Qin X, Egli M, et al. (2007) Elucidating the ticking of an in vitro circadian clockwork. *PLoS Biol* 5: 841–853.
38. Mori T, Saveliev SV, Xu Y, Stafford WF, Cox MM, et al. (2002) Circadian clock protein KaiC forms ATP-dependent hexameric rings and binds DNA. *Proc Natl Acad Sci USA* 99: 17203–17208.
39. Clodong S, Düring U, Wilde A, Axmann I, Herzel H, et al. (2007) Functioning and robustness of a bacterial circadian clock. *Mol Syst Biol* 3: 90.
40. van Zon JS, Lubensky DK, Altena PRH, Rein ten Wolde P (2007) An allosteric model of circadian KaiC phosphorylation. *Proc Natl Acad Sci USA* 104: 7420–7425.
41. Mihalcescu I, Hsing W, Leibler S (2004) Resilient circadian oscillator revealed in individual cyanobacteria. *Nature* 430: 81–85.
42. Johnson CH (2004) Precise circadian clocks in prokaryotic cyanobacteria. *Curr Issues Mol Biol* 6: 103–110.
43. Citri A, Yarden Y (2006) EGF-ERBB signalling: towards the systems level. *Nat Rev Mol Cell Biol* 7: 505–516.
44. Kitano H (2007) A robustness-based approach to systems-oriented drug design. *Drug Discov* 6: 202–210.
45. Goodwin BC (1965) Oscillatory behavior in enzymatic control processes. *Adv Enzyme Regul* 3: 425–438.
46. Ruoff P, Rensing L (1996) The temperature-compensated Goodwin model simulates many circadian clock properties. *J theor Biol* 179: 275–285.
47. Nishiwaki T, Satomi Y, Kitayama Y, Terauchi K, Kiyohara R, et al. (2007) A sequential program of dual phosphorylation of KaiC as a basis for circadian rhythm in cyanobacteria. *EMBO J* 26: 4029–4037.
48. Pattanayek R, Williams DR, Pattanayek S, Mori T, Johnson CH, et al. (2008) Structural model of the circadian clock KaiB-KaiC complex and mechanism for modulation of KaiC phosphorylation. *EMBO J* 27: 1767–1778.
49. Kitayama Y, Iwasaki H, Nishiwaki T, Kondo T (2003) KaiB functions as an attenuator of KaiC phosphorylation in the cyanobacterial circadian clock system. *EMBO J* 22: 2127–2134.
50. Gillespie DT (1977) Exact stochastic simulation of coupled chemical reactions. *J Phys Chem* 81: 2340–2361.
51. Ljung L, Glad T (1994) On global identifiability for arbitrary model parametrizations. *Automatica* 30: 265–276.
52. Daniels BC, Chen YJ, Sethna JP, Gutenkunst RN, Myers CR (2008) Slowness, robustness, and evolvability in systems biology. *Curr Opin Biotechnol* 19: 389–395.
53. Wagner A (2005) Circuit topology and the evolution of robustness in two-gene circadian oscillators. *Proc Natl Acad Sci USA* 102: 11775–11780.
54. Kitayama Y, Nishiwaki T, Terauchi Y, Kazuki (2008) Dual KaiC-based oscillations constitute the circadian system of cyanobacteria. *Genes Dev* 22: 1513–1521.
55. Francois P, Hakim V (2004) Design of genetic networks with specified functions by evolution in silico. *Proc Natl Acad Sci USA* 101: 580–585.
56. Hastings MH (2000) Circadian clockwork: two loops are better than one. *Nat Rev Neurosci* 1: 143–146.
57. Wagner A (2005) *Robustness and Evolvability in Living Systems*. Princeton: Princeton University Press.
58. Press WH, Teukolsky SA, Vetterling WS, Flannery BP (1992) *Numerical Recipes in C*. Cambridge: Cambridge University Press, 2nd edition.
59. Hoeffding W (1963) Probability inequalities for sums of bounded random variables. *J Am Stat Assoc* 58: 13–30.
60. Kageyama H, Nishiwaki T, Nakajima M, Iwasaki H, Oyama T, et al. (2006) Cyanobacterial circadian pacemaker: Kai protein complex dynamics in the KaiC phosphorylation cycle in vitro. *Mol Cell* 23: 161–171.
61. Vilar JMG, Yuan Kueh H, Barkai N, Leibler S (2002) Mechanisms of noise-resistance in genetic oscillators. *Proc Natl Acad Sci USA* 99: 5988–5992.